arXiv:1607.06616v1 [quant-ph] 22 Jul 2016

Avalanche of entanglement and correlations at quantum phase transitions

Konstantin V. Krutitsky, Andreas Osterloh, and Ralf Schützhold
Institut für Theoretische Physik, Universität Duisburg-Essen, D-47048 Duisburg, Germany.

We study the ground-state entanglement in the quantum Ising model with nearest neighbor ferromagnetic coupling J and find a sequential increase of entanglement depth with growing J. This entanglement avalanche starts with two-point entanglement, as measured by the concurrence, and continues via the three-tangle and four-tangle, until finally, deep in the ferromagnetic phase for $J = \infty$, arriving at pure ℓ-partite (GHZ type) entanglement of all ℓ spins. Comparison with the two, three, and four-point correlations reveals a similar sequence and shows strong ties to the above entanglement measures for small J. However, we also find a partial inversion of the hierarchy, where the four-point correlation exceeds the three- and two-point correlations, well before the critical point is reached. Qualitatively similar behavior is also found for the Bose-Hubbard model, suggesting that this is a general feature of a quantum phase transition. This should have far reaching consequences for approximations starting from a mean-field limit.

PACS numbers: 03.67.Mn, 05.30.Jp, 05.30.Rt, 75.10.Pq

Introduction Entanglement is one of the main reasons for the complexity of quantum many-body systems in that, the more entangled a quantum system is the more complex its description becomes. As an example, let us consider ground states of lattice Hamiltonians. If we have no entanglement between the lattice sites i, the quantum state is fully separable $|\Psi\rangle = \bigotimes_i |\psi_i\rangle$ and thus quite simple. As a result, it is possible to employ a mean-field description where observables $\hat{A}_i$ and $\hat{B}_j$ at different lattice sites i and j are uncorrelated $\langle \hat{A}_i \hat{B}_j \rangle = \langle \hat{A}_i \rangle \langle \hat{B}_j \rangle$. However, except for very few special cases (mean-field limit or Kurmann-Thomas-Müller point [1, 2]), such a description is not exact. It is possible to improve this mean-field ansatz by adding some amount of entanglement. This can be achieved either directly [3] or with matrix product states [4, 5] or tree-tensor networks [6–8]. But these descriptions do only work reliably if the entanglement is bounded in a suitable way as highlightd in Refs. [9, 10].

On the other hand, many interesting phenomena in condensed matter are associated with and occur at or close to quantum critical points, where typically the entanglement becomes very large. As one of the simplest yet prototypical examples [11], let us consider the one-dimensional Ising model in a transverse field

$$\hat{H} = -J \sum_{i=1}^{\ell} \hat{\sigma}_i^z \hat{\sigma}_{i+1}^z - \sum_{i=1}^{\ell} \hat{\sigma}_i^x \,, \tag{1}$$

where $\hat{\sigma}_i^{x,y,z}$ denote the spin-$1/2$ Pauli matrices acting on the lattice site i and periodic boundary conditions $\sigma_{\ell+1}^z = \sigma_1^z$ are imposed. This model displays a $\mathbb{Z}_2$ symmetry corresponding to the simultaneous flip of all ℓ spins. In this regard, for $\ell \to \infty$, we have a symmetry-breaking second-order quantum phase transition from the paramagnetic phase at $|J| < 1$ to ferromagnetism at $J > 1$ [11]. For $J = 0$, we have the separable paramagnetic state $|{\to}{\to}{\to}\ldots\rangle$ without entanglement while for $J \to \infty$, the ground state corresponds to the ferromagnetic state $(|{\uparrow}{\uparrow}{\uparrow}\ldots\rangle + |{\downarrow}{\downarrow}{\downarrow}\ldots\rangle)/\sqrt{2}$ with GHZ-type multi-partite entanglement between all ℓ spins. Here, $|{\to}\rangle$ is the eigenstate of σ^x and $|{\uparrow}\rangle$ that of σ^z to the eigenvalue $+1$.

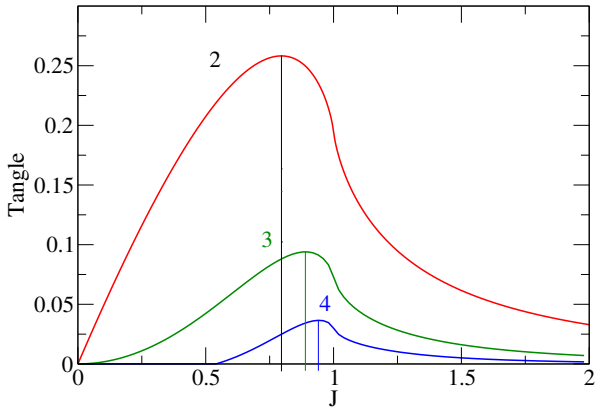

FIG. 1: (color online) The entanglement between two, three, and four neighboring spins measured by the concurrence C_2 (black), the three-tangle $\sqrt{\tau_3}$ (green), and the four-tangle τ_4 (blue) as a function of J. For the latter two, the approximation (2) was used. The concurrence starts linearly for small J and the three-tangle $\sqrt{\tau_3}$ quadratic, while the four-tangle vanishes until $J_0 \approx 0.55$. They assume their maximum values at $J_2^{\max} \approx 0.796$, $J_3^{\max} \approx 0.890$, and $J_4^{\max} \approx 0.94$, respectively – which shows the sequential increase of entanglement depth (avalanche of entanglement).

At the critical point $J_{\rm crit} = 1$, the entanglement entropy between the left and the right half of the Ising chain diverges as $\ln \ell$ [12].

However, this large amount of entanglement cannot be explained by entanglement of pairs alone [13], as measured by the concurrence. Together with the entanglement monogamy relation [14, 15] (see also [16–19]) this strongly suggests the emergence of multipartite entanglement [20, 21] (triples and quadruples etc.), which will be studied in the following section, see also Fig. 1. The relation to multipartite quantum correlations will be analyzed later on, also with reference to another prototypical model of quantum phase transitions, the Bose-Hubbard model.

Entanglement In order to study the multi-partite entanglement during the quantum phase transition of the Ising model, we employ its exact solution via Jordan-Wigner and

Bogoliubov transformation to a free fermionic model [22, 23] which allows us to obtain the reduced density matrices of two $\hat{\rho}_2 = \hat{\rho}_{ij}$, three $\hat{\rho}_3 = \hat{\rho}_{ijk}$, and four $\hat{\rho}_4 = \hat{\rho}_{ijkl}$ neighboring spins [20, 22]. After diagonalizing these matrices, we find that they all possess two dominant eigenvalues p_1 and p_2 while the sum of the remaining sub-dominant eigenvalues stays below 2.5% (for details, see the supplement [24]). Thus, we approximate the two-point reduced density operators as

$$\hat{\rho}_{ij} \approx p_1 \left|\psi^1_{ij}\right\rangle \left\langle\psi^1_{ij}\right| + (1-p_1) \left|\psi^2_{ij}\right\rangle \left\langle\psi^2_{ij}\right| \ , \qquad (2)$$

and analogously for $\hat{\rho}_{ijk}$ and $\hat{\rho}_{ijkl}$. Actually, the accuracy of this approximation should be even better than 2.5%: while the multi-partite entanglement of the first $\left|\psi^1_{\ldots}\right\rangle$ and the second $\left|\psi^2_{\ldots}\right\rangle$ eigenvectors can interfere destructively with each other, we checked that this is not the case for the third. The third eigenvector $\left|\psi^3_{\ldots}\right\rangle$ has a different structure: For three and four spins, the state(s) of the central spin(s) are fixed to $|{\rightarrow}\rangle$ while the two boundary spins form a Bell state – i.e., $\left|\psi^3_{\ldots}\right\rangle$ contains bi-partite entanglement only, which here does not interfere with the multi-partite entanglement of $\left|\psi^1_{\ldots}\right\rangle$ and $\left|\psi^2_{\ldots}\right\rangle$. As a result, we expect that the accuracy of this approximation is around 0.5% or even better. For two spins, we checked this approximation by comparing the exact concurrence with that derived from (2) and found that they are virtually indistinguishable (see the supplement [24]).

The approximation (2) as motivated by the dominance of the two largest eigenvalues is a great simplification, because we obtain rank-two density matrices, for which the three-tangle τ_3 and the four-tangle(s) τ_4 can be calculated exactly [25, 26] for this model. Note that an exact extension to arbitrary mixed states by the convex roof is not known so far for the three-tangle since the homogeneity degree of the polynomial measure is larger than two.

In analogy to the three-tangle τ_3, we call those polynomial SL-invariants that are zero for arbitrary product states [27] four-tangle and use the notation $\tau_4^{(i)}$, $i = 1, 2, 3$, for those powers that scale linearly in the density matrix. All three of them essentially lead to the same output, and therefore τ_4 will represent the four-partite entanglement content of the model. This four-partite entanglement is hence of GHZ-type because only the GHZ entanglement is measured by all three measures in the same way [27–29]. Altogether, these quantities τ_3 and τ_4 measure the tri-partite entanglement of $\hat{\rho}_3$ and the quadri-partite entanglement of $\hat{\rho}_4$, and are shown in Fig. 1. We plotted $\tau_3^{1/2}$ because this quantity also yields a homogeneous functions of degree one in the density matrix $\hat{\rho}_3$ and thus all the tangles shown have properties similar to probabilities. For completeness, we also included the pairwise entanglement of nearest neighbors, as measured by the concurrence C_2.

As is well-known, the concurrence first grows as a function of J until it reaches a maximum at $J \approx 0.796$ and later decreases again (with an infinite slope at the critical point [30]). The three-tangle $\sqrt{\tau_3}$ starts to grow much slower at small J and reaches its maximum later than the concurrence at $J \approx 0.89$. The four-tangle(s) τ_4 are even zero until $J \approx 0.55$ and reach their maximum yet a bit later at $J \approx 0.94$. Even though having no results for more spins, we conjecture that this sequence or avalanche of entanglement continues until finally, deep in the ferromagnetic phase, we get pure ℓ-partite entanglement of all spins [31].

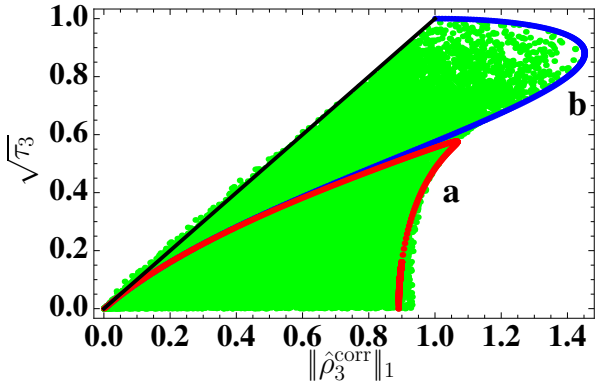

FIG. 2: (color online) Plot of the three-tangle $\sqrt{\tau_3}$ versus the three-point correlation bound $||\rho_3^{\rm corr}||_1$ for a random selection of 40.000 pure Acin states [32]. Each dot in the figure corresponds to a single state. The thin black line corresponds to $\sqrt{\tau_3} = \|\hat{\rho}_3^{\rm corr}\|_1$. The lower red (a) and upper blue curve (b) are obtained for GHZ states that are made of two $(\alpha|{\uparrow\uparrow\uparrow}\rangle + \beta|{\downarrow\downarrow\downarrow}\rangle)$ and four $(\alpha|{\uparrow\uparrow\uparrow}\rangle + \beta|\mathrm{W}\rangle)$ product basis elements, respectively, where $|W\rangle = (|{\downarrow\uparrow\uparrow}\rangle + |{\uparrow\downarrow\uparrow}\rangle + |{\uparrow\uparrow\downarrow}\rangle)/\sqrt{3}$. Although $||\rho_3^{\rm corr}||_1$ is not always larger than $\sqrt{\tau_3}$ (as it is the case for two spins), it is however satisfied approximately.

Entanglement versus correlations As already mentioned in the Introduction, a pure state without any entanglement is fully separable $|\Psi\rangle = \bigotimes_i |\psi_i\rangle$ and thus quite simple. For example, observables $\hat{A}_i$ and $\hat{B}_j$ at different lattice sites i and j are uncorrelated $\langle\hat{A}_i\hat{B}_j\rangle = \langle\hat{A}_i\rangle\langle\hat{B}_j\rangle$. In the following, we shall study the relation between entanglement and the resulting correlations in more detail. To this end, we start with the reduced density matrices for one $\hat{\rho}_1 = \hat{\rho}_i$, two $\hat{\rho}_2 = \hat{\rho}_{ij}$, three $\hat{\rho}_3 = \hat{\rho}_{ijk}$, and four $\hat{\rho}_4 = \hat{\rho}_{ijkl}$ spins and split up the correlated parts via $\hat{\rho}_{ij}^{\rm corr} = \hat{\rho}_{ij} - \hat{\rho}_i\hat{\rho}_j$, and analogously for more spins (see supplement [24]). The correlation between the two observables $\langle\hat{A}_i\hat{B}_j\rangle^{\rm corr} = \langle\hat{A}_i\hat{B}_j\rangle - \langle\hat{A}_i\rangle\langle\hat{B}_j\rangle$ can be written as $\langle\hat{A}_i\hat{B}_j\rangle^{\rm corr} = \mathrm{Tr}\{\hat{A}_i\hat{B}_j\hat{\rho}_{ij}^{\rm corr}\}$ and similarly for three or more sites.

Since correlations such as $\langle\hat{A}_i\hat{B}_j\rangle^{\rm corr}$ and $\langle\hat{A}_i\hat{B}_j\hat{C}_k\rangle^{\rm corr}$ obviously depend on the observables $\hat{A}_i$, $\hat{B}_j$, and $\hat{C}_k$, it is convenient to derive an estimate directly from the correlated density matrices such as $\hat{\rho}_{ij}^{\rm corr}$. For observables whose norm is bounded by unity ($|\hat{A}_i| \leq 1$, $|\hat{B}_j| \leq 1$ etc.) such as the Pauli spin matrices, we obtain

$$\begin{aligned}\langle\hat{A}_i\hat{B}_j\rangle^{\rm corr} &= \mathrm{Tr}\left\{\hat{A}_i\hat{B}_j\hat{\rho}_{ij}^{\rm corr}\right\} = \sum_I \lambda_I \left\langle\chi^I_{ij}\right| \hat{A}_i\hat{B}_j \left|\chi^I_{ij}\right\rangle \\ &\leq \sum_I |\lambda_I| = ||\hat{\rho}_{ij}^{\rm corr}||_1 \, , \end{aligned} \qquad (3)$$

where we have inserted the diagonalization of $\hat{\rho}_{ij}^{\rm corr}$ with eigenvalues λ_I and eigenvectors $\left|\chi^I_{ij}\right\rangle$. We find that the Schat-

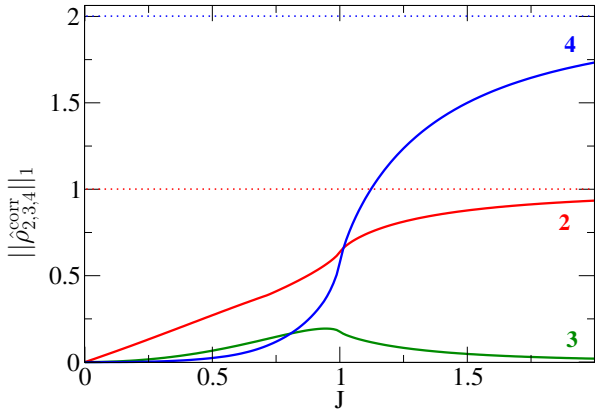

FIG. 3: (color online) Norms of correlated reduced density operators for two $\hat{\rho}_2^{\rm corr}$ (red), three $\hat{\rho}_3^{\rm corr}$ (green), and four $\hat{\rho}_4^{\rm corr}$ (blue) neighboring spins in the transverse Ising model. At $J \approx 0.8$, i.e., well before the critical point, the 4-point correlations exceed the 3-point correlations. The 2-point correlations dominate both until the critical point is reached, afterwards the 4-point correlations prevail. The horizontal dashed lines represent the asymptotic values for $J \to \infty$.

ten one-norm $||\hat{\rho}_{ij}^{\rm corr}||_1$ of the correlated density matrix $\hat{\rho}_{ij}^{\rm corr}$ yields an upper estimate for the correlations $\langle \hat{A}_i \hat{B}_j \rangle^{\rm corr}$ of all observables whose norm is bounded by unity. Hence, we shall focus on this quantity in the following. Obviously, the same argument can be applied to three or more sites in complete analogy.

For two spins, it is well-known that the largest correlation function for pure states coincides with the concurrence [33]. For mixed states, this becomes an upper bound, i.e., the maximum correlation is larger or equal to the concurrence $||\hat{\rho}_{ij}^{\rm corr}||_1 \geq C_2$. Unfortunately, for three or more spins, such a rigorous bound is not known.

Thus, let us consider a system of three spins. A pure state of the system can be represented as a superposition of five local bases product states [32]. We generate these states randomly and calculate the three-tangle τ_3 and $||\hat{\rho}_{ijk}^{\rm corr}||_1$. The results are plotted in Fig. 2. Again, we show $\sqrt{\tau_3}$ because this quantity is a homogeneous function of degree one in the density operator $\hat{\rho}_3$ and thus has properties similar to a probability. We find that $\sqrt{\tau_3}$ is a very good approximation for a lower bound to $||\hat{\rho}_{ijk}^{\rm corr}||_1$. This is very similar to the two-spin case above, but one should be aware that $\sqrt{\tau_3}$ can exceed $||\hat{\rho}_{ijk}^{\rm corr}||_1$ a little bit – there are points in Fig. 2 which lie slightly on the left of the black diagonal line (indicating the points where $||\hat{\rho}_{ijk}^{\rm corr}||_1 = \sqrt{\tau_3}$).

Similar calculations for four spins indicate that $||\hat{\rho}_{ijkl}^{\rm corr}||_1$ is also an approximate upper bound for the four-tangle τ_4. However, since the available phase space for four spins is much larger, the statistics is rather poor (see more details in the supplement [24]).

In summary, while the two-point correlation $\hat{\rho}_{ij}^{\rm corr}$ and the pairwise entanglement C_2 are related via the *exact* bound $||\hat{\rho}_{ij}^{\rm corr}||_1 \geq C_2$, we find analogous approximate relations between the three- and four-point correlations $\hat{\rho}_{ijk}^{\rm corr}$ and $\hat{\rho}_{ijkl}^{\rm corr}$ on the one hand and the corresponding entanglement measures $\sqrt{\tau_3}$ and τ_4 on the other hand.

Correlations for the Ising model Motivated by the above findings, let us study the Schatten one-norms of the correlated density matrices for two, three, and four neighboring spins. Note that we used the exact results for the reduced density matrices (obtained by Jordan-Wigner and Bogoliubov transformation) without the approximation (2). The results are plotted in Fig. 3. As expected from stationary perturbation theory (see supplement), the two-point correlation $||\hat{\rho}_2^{\rm corr}||_1 = ||\hat{\rho}_{ij}^{\rm corr}||_1$ behaves linearly in J for small J, while the three-point correlation $||\hat{\rho}_3^{\rm corr}||_1 = ||\hat{\rho}_{ijk}^{\rm corr}||_1$ and the four-point correlation $||\hat{\rho}_4^{\rm corr}||_1 = ||\hat{\rho}_{ijkl}^{\rm corr}||_1$ scale with the second and third power of J, respectively.

Thus, for small J, the correlations obey the same hierarchy $||\hat{\rho}_2^{\rm corr}||_1 \gg ||\hat{\rho}_3^{\rm corr}||_1 \gg ||\hat{\rho}_4^{\rm corr}||_1$ as the entanglement measures in Fig. 1, except that $||\hat{\rho}_4^{\rm corr}||_1$ does not vanish for finite J in contrast to τ_4. However, at $J \approx 0.8$, i.e., well before the critical point, this hierarchy is violated as the four-point correlation $||\hat{\rho}_4^{\rm corr}||_1$ exceeds the three-point correlation $||\hat{\rho}_3^{\rm corr}||_1$. The two-point correlation $||\hat{\rho}_2^{\rm corr}||_1$ is still dominant in this region – this only changes near the critical point. This inversion of the hierarchy, i.e., the dominance of $||\hat{\rho}_4^{\rm corr}||_1$ over $||\hat{\rho}_3^{\rm corr}||_1$ in a region within the symmetric paramagnetic phase, should be relevant for approximation schemes which truncate the hierarchy of correlations at some order (see below).

Bose-Hubbard model One might suspect that this inversion of the hierarchy is a rather specific result due to the integrability of the model under consideration or may be induced by the fact that deep in the ferromagnetic (broken-symmetry) phase, the three-point correlation vanishes whereas the four-point (and two-point) correlators approach constant non-zero values. (Note that an inversion of the two-point and four-point correlations just happens at the critical point.) In order to investigate whether the inversion of the hierarchy is a general phenomenon or indeed a peculiar feature of the Ising model, let us consider the other prototypical example for a quantum phase transition [11, 34], the Bose-Hubbard model

$$\hat{H} = -J \sum_{i=1}^{\ell} \left(\hat{b}_i^\dagger \hat{b}_{i+1} + \hat{b}_{i+1}^\dagger \hat{b}_i \right) + \frac{1}{2} \sum_{i=1}^{\ell} \hat{b}_i^\dagger \hat{b}_i^\dagger \hat{b}_i \hat{b}_i \qquad (4)$$

that is believed to be non-integrable [35–38]. Here $\hat{b}_i^\dagger$ and $\hat{b}_i$ are the bosonic creation and annihilation operators at the lattice site i. As before, we impose periodic boundary conditions. Note that the hopping rate J is dimensionless because we measure it in units of the on-site interaction energy (usually denoted by U).

At unit filling $\langle \hat{n}_i \rangle = 1$, there is a quantum phase transition (in the thermodynamic limit $\ell \to \infty$) between the Mott insulator regime where the on-site repulsion dominates (in analogy to the paramagnetic state for the Ising model) and the superfluid phase where the hopping rate J dominates (analogously to the ferromagnetic state). Deep in the Mott phase at $J = 0$, the ground state factorizes $|\Psi\rangle = \bigotimes_i |1\rangle_i$, i.e., it is not entangled. For increasing J, on the other hand, we get correlations

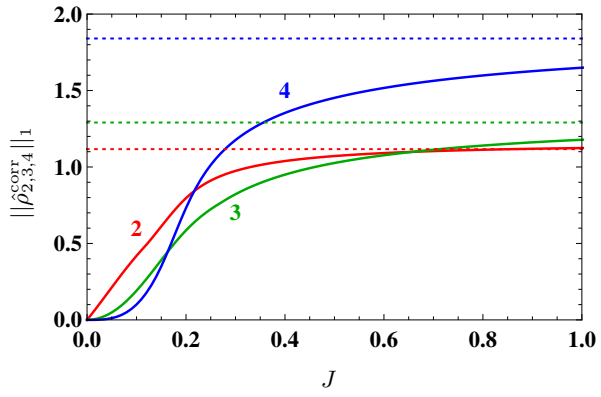

FIG. 4: (color online) Norms of correlated reduced density operators for two $\hat{\rho}_2^{\rm corr}$ (red), three $\hat{\rho}_3^{\rm corr}$ (green), and four $\hat{\rho}_4^{\rm corr}$ (blue) neighboring sites in the Bose-Hubbard model with 12 particles in 12 lattices sites. The horizontal dotted lines represent the limit of the ideal Bose gas (superfluid phase $J \to \infty$). We see qualitatively similar features as for the Ising model, except that the three-point correlation is monotonically increasing. The initial sequence (first two-point, later three-point and even later four-point correlations) is also present in this case. Again, the four-point correlations overtake the three-point correlations well before the critical point (here around $J_{\rm crit} \approx 0.3$).

such as $\langle \hat{b}_i^\dagger \hat{b}_j \rangle$ which are somewhat analogous to the ferromagnetic correlations $\langle \hat{\sigma}_i^z \hat{\sigma}_j^z \rangle$.

Unfortunately, for the Bose-Hubbard model, entanglement measures in analogy to the concurrence are not yet available. There exist genuine bi-partite and multi-partite entanglement measures for bosons, but they are known only for special cases such as Gaussian states or suitable pure states (see [39, 40] and references therein). Hence, we focus on the reduced density matrices and their correlated parts. We consider a system of finite size (12 bosons on 12 lattice sites) and obtain the ground state numerically for arbitrary J by exact diagonalization in the subspace of the Hilbert space where the total momentum is zero. This allows to calculate exactly the reduced density matrices. We find that they contain, in contrast to the Ising model, in general more than two non-negligible eigenvalues, i.e., the approximation (2) would not apply here.

In analogy to Fig. 3, we plot the Schatten one-norms of the correlated parts of the reduced density matrices in Fig. 4. We find that – again in contrast to the Ising model – all three curves are monotonically growing and approach finite asymptotic values for $J \to \infty$ which correspond to the limit of a free (ideal) Bose gas and can be calculated analytically. Similarly to the Ising model, we find $||\hat{\rho}_q^{\rm corr}||_1 \sim J^{q-1}$ with $q = 2, 3, 4$ for small J, as expected from strong-coupling perturbation theory (see Supplement [24]). This scaling imposes the hierarchy $||\hat{\rho}_2^{\rm corr}||_1 \gg ||\hat{\rho}_3^{\rm corr}||_1 \gg ||\hat{\rho}_4^{\rm corr}||_1$ at small values of J. However, in analogy to the Ising model, this hierarchy is partially inverted at $J \approx 0.16$ and $J \approx 0.21$, i.e. both well before the critical point is reached (here around $J_{\rm crit} \approx 0.3$, see Ref. [41] for a recent review).

Conclusions For the Ising model (1), we study the entanglement of two, three, and four neighbouring sites in the ground state by means of the approximation (2) based on the dominance of two eigenvalues. We find a sequential increase of entanglement depth with growing J which we call avalanche of entanglement (see Fig. 1). We conjecture that this avalanche continues until pure ℓ-partite (GHZ type) entanglement emerges for $J = \infty$. This avalanche might also explain the $\ln \ell$ divergence of the entanglement entropy at the critical point, which will be subject of future work.

Using the Schatten one-norms of the correlated reduced density matrices as rigorous upper bounds for the correlations (3), we find that they also yield approximate upper bounds for the corresponding entanglement measures (see Fig. 2). As expected from these observed strong ties between entanglement and correlations, we find that the latter display a similar sequence (first two-point, later three-point and even later four-point correlations) when increasing J (see Fig. 3). However, we also find a partial inversion of the hierarchy of correlations: at $J \approx 0.8$, i.e., well before the critical point $J_{\rm crit} = 1$ is reached, the four-point correlations exceed the three-point correlations and eventually also the two-point correlations. Comparison with the Bose-Hubbard model as another prototypical example reveals a qualitatively similar behavior, including the partial inversion of the hierarchy of correlations at $J \approx 0.16$, i.e., well before the critical point at $J_{\rm crit} \approx 0.3$.

This inversion of the hierarchy is relevant for approximation schemes based on truncation [42–48]. Let us consider a quantity such as $\langle \sigma_i^x \sigma_j^x \sigma_k^x \sigma_l^x \rangle$. To lowest order (mean-field limit), one could approximate it via $\langle \sigma_i^x \sigma_j^x \sigma_k^x \sigma_l^x \rangle \approx \langle \sigma_i^x \rangle \langle \sigma_j^x \rangle \langle \sigma_k^x \rangle \langle \sigma_l^x \rangle$, i.e., by neglecting all correlations. As a possible first-order correction, one could include two-point correlations such as $\langle \sigma_i^x \sigma_j^x \rangle^{\rm corr} \langle \sigma_k^x \rangle \langle \sigma_l^x \rangle$. This first-order approximation allows us to derive e.g. the magnon dispersion relations. One can try to successively improve the accuracy of this approximation by shifting the truncation, i.e., by including more and more higher-order correlations. While this successive approximation procedure works well for small J, we found here that it fails for larger J, even well before reaching the critical point.

Outlook It might be interesting to study the possibility of more general approximation schemes such as (2) based on the dominance of two or more eigenvalues of the reduced density operator. In a time-dependent setting one could analyze how this entanglement avalanche is affected by non-adiabatic dynamics during a sweep through the critical point.

This work was supported by the SFB 1242 of the German Research Foundation (DFG).

[1] J. Kurmann, H. Thomas, and G. Müller, Physica A **112**, 235 (1982).
[2] S. M. Giampaolo, G. Adesso, and F. Illuminati, Phys. Rev. B **79**,

224434 (2009).
[3] A. Osterloh and R. Schützhold, Phys. Rev. B **91**, 125114 (2015).
[4] F. Vertraete, V. Murg, and J. I. Cirac, Adv. Phys. **57**, 143 (2008).
[5] F. Verstraete and J. I. Cirac, Phys. Rev. Lett. **104** (2010).
[6] I. Pižorn, F. Verstraete, and R. M. Konik, Phys. Rev. B **88**, 195102 (2013).
[7] L. Tagliacozzo, G. Evenbly, and G. Vidal, Phys. Rev. B **80**, 235127 (2009).
[8] Y.-Y. Shi, L.-M. Duan, and G. Vidal, Phys. Rev. A **74**, 022320 (2006).
[9] G. Vidal, Phys. Rev. Lett. **91**, 147902 (2003).
[10] However, one should be aware that the criterion in Ref. [9] does not apply in most relevant cases, where the rank of the reduced density matrix is maximal and consequently the guaranteed upper bound would scale exponentially with the system size. Thus, its application requires approximations such as (2).
[11] S. Sachdev, *Quantum Phase Transition* (Cambridge University Press, 1999).
[12] G. Vidal, J. Latorre, E. Rico, and A. Kitaev, Phys.Rev. Lett. **90**, 227902 (2003).
[13] L. Amico, A. Osterloh, F. Plastina, G. Palma, and R. Fazio, Phys. Rev. A **69**, 022304 (2004).
[14] V. Coffman, J. Kundu, and W. K. Wootters, Phys. Rev. A **61**, 052306 (2000).
[15] T. J. Osborne and F. Verstraete, Phys. Rev. Lett. **96**, 220503 (2006).
[16] B. Regula, S. D. Martino, S. Lee, and G. Adesso, Phys. Rev. Lett. **113**, 110501 (2014).
[17] B. Regula, S. D. Martino, S. Lee, and G. Adesso, Phys. Rev. Lett. **116**, 049902 (2016), erratum.
[18] B. Regula and G. Adesso, Phys. Rev. Lett. **116**, 070504 (2016).
[19] B. Regula, A. Osterloh, and G. Adesso (2016), arXiv:1604.03419.
[20] M. Hofmann, A. Osterloh, and O. Gühne, Phys. Rev. B **89**, 134101 (2014).
[21] A. Osterloh, Phys. Rev. A **93**, 052322 (2016).
[22] P. Pfeuty, Ann.Phys. **57**, 79 (1970).
[23] E. Lieb, T. Schultz, and D. Mattis, Ann. Phys. **16**, 407 (1961).
[24] See Supplemental Material at [URL will be inserted by publisher] for details.
[25] R. Lohmayer, A. Osterloh, J. Siewert, and A. Uhlmann, Phys. Rev. Lett. **97**, 260502 (2006).
[26] A. Osterloh, J. Siewert, and A. Uhlmann, Phys. Rev. A **77**, 032310 (2008).
[27] A. Osterloh and J. Siewert, Phys. Rev. A **72**, 012337 (2005).
[28] A. Osterloh and J. Siewert, Int. J. Quant. Inf. **4**, 531 (2006).
[29] D. Ž. Đoković and A. Osterloh, J. Math. Phys. **50**, 033509 (2009).
[30] A. Osterloh, L. Amico, G. Falci, and R. Fazio, Nature **416**, 608 (2002).
[31] This feature survives taking into consideration that we only solve the Hamitonian for an odd number of excitations.
[32] A. Acín, A. Andrianov, E. Jane, and R. Tarrach, J. Phys. A **34**, 6725 (2001).
[33] F. Verstraete, M. Popp, and J. Cirac, Phys. Rev. Lett. **92**, 027901 (2004).
[34] M. Lewenstein, A. Sanpera, and V. Ahufinger, *Ultracold Atoms in Optical Lattices: Simulating quantum many-body systems* (Oxford University Press, 2012).
[35] A. Buchleitner and A. R. Kolovsky, Phys. Rev. Lett. **91**, 253002 (2003), URL http://link.aps.org/doi/10.1103/PhysRevLett.91.253002.
[36] A. R. Kolovsky and A. Buchleitner, EPL (Europhysics Letters) **68**, 632 (2004), URL http://stacks.iop.org/0295-5075/68/i=5/a=632.
[37] M. Hiller, T. Kottos, and T. Geisel, Phys. Rev. A **79**, 023621 (2009), URL http://link.aps.org/doi/10.1103/PhysRevA.79.023621.
[38] C. Kollath, G. Roux, G. Biroli, and A. M. Läuchli, Journal of Statistical Mechanics: Theory and Experiment **2010**, P08011 (2010), URL http://stacks.iop.org/1742-5468/2010/i=08/a=P08011.
[39] L. Amico, R. Fazio, A. Osterloh, and V. Vedral, Rev. Mod. Phys. **80**, 517 (2008).
[40] F. Holweck and P. Lévay, J. Phys. A **49**, 085201 (2016).
[41] K. V. Krutitsky, Physics Reports **607**, 1 (2016), ISSN 0370-1573, ultracold bosons with short-range interaction in regular optical lattices, URL http://www.sciencedirect.com/science/article/pii/S0370157315004366.
[42] K. G. Moter and R. S. Fishman, Phys. Rev. B **45**, 5307 (1992), URL http://link.aps.org/doi/10.1103/PhysRevB.45.5307.
[43] R. S. Fishman and S. H. Liu, Phys. Rev. B **45**, 5406 (1992), URL http://link.aps.org/doi/10.1103/PhysRevB.45.5406.
[44] J. Jensen, Phys. Rev. B **49**, 11833 (1994), URL http://link.aps.org/doi/10.1103/PhysRevB.49.11833.
[45] F. Queisser, P. Navez, and R. Schützhold, Phys. Rev. A **85**, 033625 (2012).
[46] P. Navez, F. Queisser, and R. Schützhold, J. Phys. A **47**, 225004 (2014).
[47] F. Queisser, K. Krutitsky, P. Navez, and R. Schützhold, Phys. Rev. A. **89**, 033616 (2014).
[48] K. V. Krutitsky, P. Navez, F. Queisser, and R. Schützhold, EPJ Quantum Technology **1**, 1 (2014), ISSN 2196-0763, URL http://dx.doi.org/10.1140/epjqt12.

Supplemental material to
Avalanche of entanglement and correlations at quantum phase transitions

Here we report on additional material that supports findings of the main paper.

ENTANGLEMENT MEASURES AND CORRELATION FUNCTIONS

Correlated reduced density operators

We consider the Hamiltonian for a system of L lattice sites of the form

$$\hat{H} = \sum_{\ell_1 \neq \ell_2} \hat{H}_{\ell_1 \ell_2} + \sum_{\ell} \hat{H}_{\ell} \, , \tag{S1}$$

where $\hat{H}_{\ell}$ and $\hat{H}_{\ell_1 \ell_2}$ are local and two-site operators, respectively; the indices label the lattice sites. The state of the whole system can be described by the density operator $\hat{\rho} = |\psi\rangle\langle\psi|$. In order to study parts of the system, we introduce reduced density operators for q lattice sites via averaging (partially tracing) over all other sites:

$$\hat{\rho}_{\ell_1 \ldots \ell_q} = \mathrm{Tr}_{\ell_{q+1} \ldots \ell_L} \hat{\rho} \, , \tag{S2}$$

where all $\ell_1, \ldots, \ell_L \, : \, \{1, \ldots, L\}$ are distinct. Information about all possible spatial correlations of the lattice sites $\ell_1 \ldots \ell_q$ is directly contained in the correlated parts of the reduced density operator $\hat{\rho}^{\mathrm{corr}}_{\ell_1 \ldots \ell_q}$. They are constructed in the same manner as cumulants. For $q = 2, 3$ they are explicitly given by

$$\begin{aligned} \hat{\rho}^{\mathrm{corr}}_{\ell_1 \ell_2} &= \hat{\rho}_{\ell_1 \ell_2} - \hat{\rho}_{\ell_1} \hat{\rho}_{\ell_2} \\ \hat{\rho}^{\mathrm{corr}}_{\ell_1 \ell_2 \ell_3} &= \hat{\rho}_{\ell_1 \ell_2 \ell_3} - \hat{\rho}^{\mathrm{corr}}_{\ell_1 \ell_2} \hat{\rho}_{\ell_3} - \hat{\rho}^{\mathrm{corr}}_{\ell_1 \ell_3} \hat{\rho}_{\ell_2} - \hat{\rho}^{\mathrm{corr}}_{\ell_2 \ell_3} \hat{\rho}_{\ell_1} \\ &\quad - \hat{\rho}_{\ell_1} \hat{\rho}_{\ell_2} \hat{\rho}_{\ell_3} \, . \end{aligned} \tag{S3}$$

The operators $\hat{\rho}^{\mathrm{corr}}_{\ell_1 \ldots \ell_q}$ are hermitean and their traces vanish: $\mathrm{Tr} \hat{\rho}^{\mathrm{corr}}_{\ell_1 \ldots \ell_q} = 0$. They allow to calculate (connected) correlation functions of local operators $\hat{O}_{\ell}$ as

$$\langle \hat{O}_{\ell_1} \ldots \hat{O}_{\ell_q} \rangle^{\mathrm{corr}} = \mathrm{Tr} \left(\hat{\rho}^{\mathrm{corr}}_{\ell_1 \ldots \ell_q} \hat{O}_{\ell_1} \ldots \hat{O}_{\ell_q} \right) \, . \tag{S4}$$

In order to obtain quantitative estimates of the q-point correlations, it is convenient to consider the Schatten p-norms

$$||\hat{\rho}^{\mathrm{corr}}_{\ell_1 \ldots \ell_q}||_p := \sqrt[p]{\mathrm{Tr}|\hat{\rho}^{\mathrm{corr}}_{\ell_1 \ldots \ell_q}|^p} \equiv \left(\sum_i |\lambda^{(i)}_{\ell_1 \ldots \ell_q}|^p \right)^{1/p} \, , \tag{S5}$$

where $\lambda^{(i)}_{\ell_1 \ldots \ell_q}$ are the eigenvalues of the correlated density operators $\hat{\rho}^{\mathrm{corr}}_{\ell_1 \ldots \ell_q}$. The Schatten one-norm is also known as the trace norm and the two-norm is often called the Frobenius norm or the Hilbert-Schmidt norm. Assuming that the aboslute value of the matrix elements $\langle i|\hat{O}_{\ell_1} \ldots \hat{O}_{\ell_q}|i\rangle$ in the eigenstates $|i\rangle$ of the operator $\hat{\rho}^{\mathrm{corr}}_{\ell_1 \ldots \ell_q}$ are not larger than one, it is easy to see that $\left| \langle \hat{O}_{\ell_1} \ldots \hat{O}_{\ell_q} \rangle^{\mathrm{corr}} \right| \leq ||\hat{\rho}^{\mathrm{corr}}_{\ell_1 \ldots \ell_q}||_1$.

In the present work, we deal with the ground states of one-dimensional translationally invariant systems. In this case, the density matrices depend only on the distances between the lattices sites. One can always order the site indices such that $\ell_1 < \ell_2 < \cdots < \ell_q$ and we can write $\hat{\rho}^{\mathrm{corr}}_{\ell_1 \ldots \ell_q} \equiv \hat{\rho}^{\mathrm{corr}}_{q}(d_1, \ldots, d_{q-1})$, where $d_i = \ell_{i+1} - \ell_i > 0$ are the corresponding distances. Intuitively, one would expect that (i) the correlations of a fixed number of sites decrease with the distances between the sites and (ii) the correlations for fixed distances decrease with the number of sites. For nearest neighbors, the latter would lead to inequalities

$$||\hat{\rho}^{\mathrm{corr}}_2(1)||_p \gg ||\hat{\rho}^{\mathrm{corr}}_3(1,1)||_p \gg \ldots \tag{S6}$$

Our analysis of two completely different models presented below shows that the expectation (i) is always satisfied whereas (ii) does not necessarily hold.

Correlations as upper bounds to entanglement

For pure states, the largest correlation function $||\hat{\rho}^{\mathrm{corr}}_{\ell_1 \ell_2}||_1$ coincides with the concurrence $C_2(\ell_1, \ell_2)$ [1]. This strict equality for pure states turns into an upper bound for the concurrence of mixed states (see Fig. S1). It is interesting to see whether the respective correlation functions are an upper bound to the corresponding entanglement measure.

For the three-tangle τ_3 we find that it is almost upper bounded by $\|\hat{\rho}^{\mathrm{corr}}_3\|_1$ for pure states of three qubits (see Fig. S2 or Fig. 2 in the main paper). There are however some pure states for which τ_3 is slighly above $\|\hat{\rho}^{\mathrm{corr}}_3\|_1$.

We do not reach a satisfactory statistics to make a similar statement also in the situation of pure states for four qubits. The result is shown for 900.000 random choices of pure states for τ_4^a in Fig. S3. It can be seen, however, that for almost all states out of this sample the inequality holds; there are examples shown for which $\|\hat{\rho}^{\mathrm{corr}}_4\|_1$ is smaller than τ_4^a.

The genuine multipartite entanglement content, i.e. the three-tangle $\sqrt{\tau_3}$ and the three four-tangles $\tau_4^a = \sqrt[3]{\mathcal{F}_1^{(4)}}$, $\tau_4^b = \sqrt[4]{\left\langle \mathcal{F}_2^{(4)} \right\rangle_s}$, and $\tau_4^c = \sqrt[6]{\mathcal{F}_3^{(4)}}$ from Ref. [4] for the nearest-neighboring sites are shown in Fig. 1 of the main article. Numerical calculations show that τ_4^a, τ_4^b, τ_4^c for the nearest neighbors are the same, although we do not have a rigorous analytical proof of that. Therefore, we do not need to distinguish between the three four-tangles and drop the upper index. This also means that the entanglement would only be due to

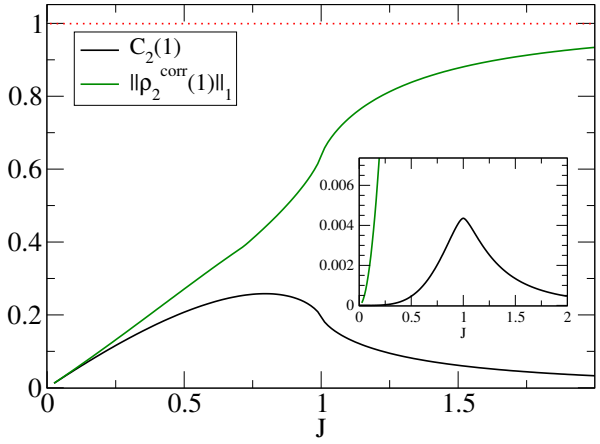

FIG. S1: The concurrence $C_2(d)$ is plotted together with $\|\rho_2^{\rm corr}(d)\|_1$ for distances $d = 1$ (left figure) and $d = 2$ (right figure). For $d = 1$, it is clearly seen that indeed $\|\rho_2^{\rm corr}(1)\|_1$ as largest correlation function is an upper bound to the corresponding concurrence. For $d = 2$, the concurrence drops to 0.04 at its maximum at the critical point, wheras $\|\rho_2^{\rm corr}(2)\|_1$ is about roughly the same as $\|\rho_2^{\rm corr}(1)\|_1$.

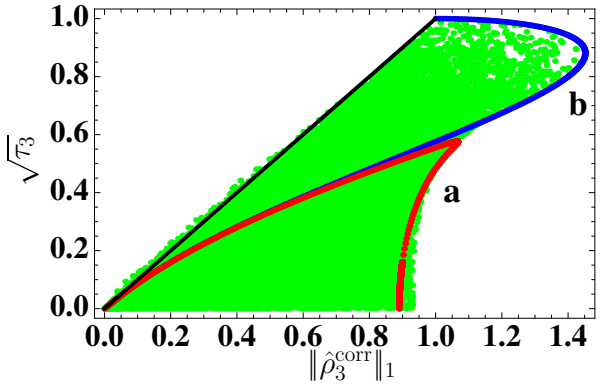

FIG. S2: The three-tangle is plotted against the largest correlation for pure states. We have done a plot for each state as labled by an Acin state [2] statistically. Each dot in the figure corresponds to a single state. Although the largest correlation function is not always larger that the three-tangle (as for two qubits) it is however satisfied approximately (see the thin black line, signalling equality of the both). The green and red curve are GHZ states which are made of two and four components, respectively. The four component GHZ state connects the W states with the product states. It is seen that some states do exist with an even larger $\|\rho_3^{\rm corr}\|_1$ as the W state.

the three- or four-particle GHZ-states, respectively. Such a behaviour goes conform with the expectations for that particular model [21].

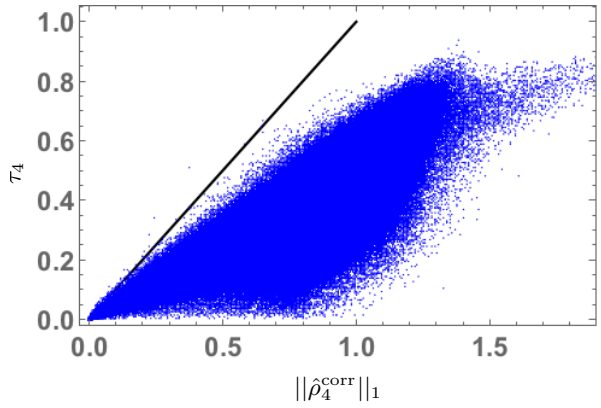

FIG. S3: The four-tangle τ_4 is shown here against $\|\hat{\rho}_4^{\rm corr}\|_1$ for pure states. We have chosen the pure states statistically from the extended Schmidt form [3]. Each dot in the figure corresponds to a single state. We do not have enough statistics, as can be seen from our viewgraph. Although states for arbitrary value of τ_4 should be there whose value of $\|\hat{\rho}_4^{\rm corr}\|_1$ comes arbitrarily close to the line $\tau_4 = \|\hat{\rho}_4^{\rm corr}\|_1$, we don't see any occurrences at larger values of τ_4.

RESULTS FOR THE ISING MODEL

Rank-two approximation

The quantum transverse Ising model is a special case of the transverse XY-model

$$\hat{H} = -J \sum_{i=1}^{\ell} \left(\frac{1+\gamma}{2} \hat{\sigma}_i^x \hat{\sigma}_{i+1}^x + \frac{1-\gamma}{2} \hat{\sigma}_i^y \hat{\sigma}_{i+1}^y \right) - \sum_{i=1}^{\ell} \hat{\sigma}_i^z \,. \tag{S7}$$

For $\gamma \neq 0$ it has a quantum phase transition of the Ising type. The reduced density matrices of two, $\hat{\rho}_2 = \hat{\rho}_{ij}$, three, $\hat{\rho}_3 = \hat{\rho}_{ijk}$, and four, $\hat{\rho}_4 = \hat{\rho}_{ijkl}$, neighboring spins [5, 6] essentially possess two dominant eigenvalues p_1 and p_2 while the sum of the remaining sub-dominant eigenvalues stays below 2.5%. The second eigenvector interferes strongly with the entanglement of the first, whereas we checked that this is not the case for the third; the remaining error is maximally $p_{I>3} \approx 0.5\%$. Therefore we only consider the case of rank two density matrices and neglect the rest of few percents of weight. What one is left with are the two highest weights p_1 and p_2 of the density matrix. We briefly discuss two ways of taking care of them: 1) take p_1 or 2) take $p_1/(p_1 + p_2)$ as the highest weight of the new rank-two density matrix. Whereas in 1) one assumes that the neglected part is as destructive to the entanglement as the second state is, in 2) the remaining states do not enter the calculation at all. Both are neither an upper bound nor a lower bound to the entanglement. Details on how the approximations works for the concurrence can be seen in Figs. S4 and S5.

The procedure 1) works perfectly for nearest neighbors, where the plots can hardly be distinguished for the transverse Ising model and also for the transverse XY-model for J up to the factorising field, where they start to deviate consid-

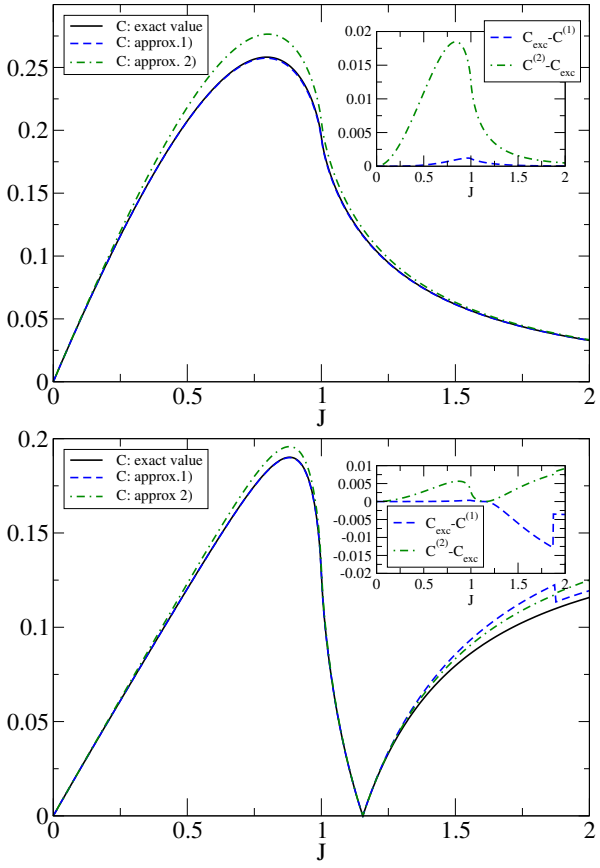

FIG. S4: Top: The concurence $C_2(1)$ is plotted together with the two approximations 1) and 2) (see text) for the transverse Ising model. It can be seen that approximation 1) (blue dashed curve; almost invisible here) basically coincides with the exact concurrence (black curve). The approximation following scheme 2) (green dash-dotted curve) slightly lies above the exact curve. This is demonstrated in the inset, where the differences $C^{(1)}_{\text{Diff.}} := C - C^{(1)}$ (blue dashed curve) and $C^{(1)}_{\text{Diff.}} := C^{(2)} - C$ (red curve) are shown. Bottom: The same plots as for the transverse Ising chain are shown here for the transverse XY model with anisotropy parameter $\gamma = 0.5$. Here the concurrence $C_2(1)$ is well described by approximation scheme 1) up to the factorising field. Beyond this point, the approximation is still reasonable, but lies above the exact curve.

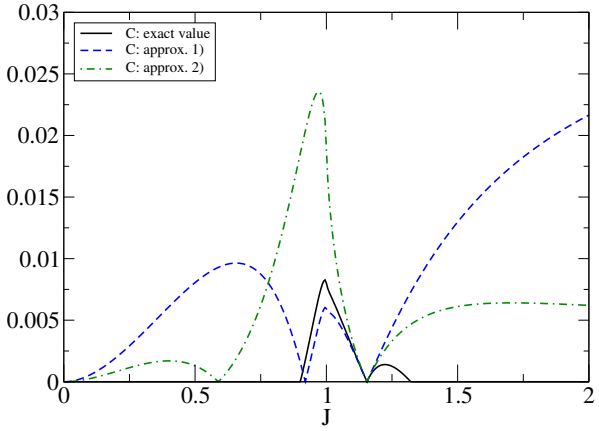

FIG. S5: The concurrence $C_2(3)$ is shown for the transverse XY-model and anisotropy parameter $\gamma = 0.5$. The approximation following scheme 1) is reasonable around the critical point in between the two zeros. Beyond these points it deviates considerably from zero. It however gives a close prediction of the non-trivial zero of $C_2(3)$.

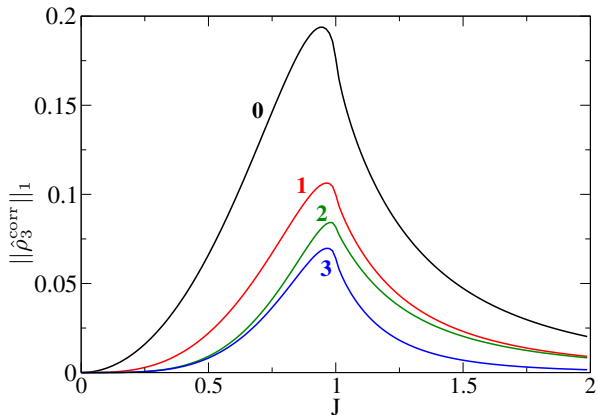

FIG. S6: $\|\hat{\rho}_3^{\text{corr}}(d_1, d_2)\|_1$ is shown for (d_1, d_2) from nearest neighbors $(1, 1)$ (black, 0) to $(1, 3)$ (green, 2) together with $(2, 2)$ (blue, 3). It is not much affected like for the two-site case, in that it only goes down to about one third of $\|\hat{\rho}_3^{\text{corr}}(1, 1)\|_1$. The maximum is assumed at roughly $J \gtrsim 0.945$ and is slighly moving towards the critical point $J_c = 1$ when the sites are moving away from each other.

erably. This is different when considering larger distances, where both curves have similar shapes only around the critical point (see Fig. S5). It gives good estimates even for the zeros of the exact concurrence and avoids over-estimating the entanglement in the state.

Correlation functions

The concurrences $C_2(\ell_1, \ell_2) \equiv C_2(d)$, where $d = |\ell_2 - \ell_1|$ are shown together with the 1-norm of ρ_2^{corr} in Fig. S1. Wheras the 1-norm of the correlations has no substantial changes, the concurrence at distance $d = 2$ modifies to about 2% of the maximal value for nearest neighbors (see inset).

This qualitatively doesn't change much for 3 sites at distances (d_1, d_2) which means that if the first particle is at site ℓ_1 the next site is at $\ell_1 + d_1$ and the third one at $\ell_1 + d_1 + d_2$ (hence, the next neighbor reduced density matrix would be $\hat{\rho}_3(1, 1)$). This is shown in Fig. S6, where different distances have been considered for $\|\hat{\rho}^{\text{corr}}(d_1, d_2)\|_1$: $(d_1, d_2) = (1, 1)$ to $(1, 3)$ and $(2, 2)$. $\|\hat{\rho}_3^{\text{corr}}(d_1, d_2)\|_1$ decays to about one third of the nearest neighbor situation $\|\hat{\rho}_3^{\text{corr}}(1, 1)\|_1$ with a maximum at $J \gtrsim 0.945$ which is moving tinily up to 0.98. One could extract the tendency that the maximum moves for $(1, 1)$ to $(1, d_2)$ and from $(1, 1)$ to (d_1, d_1) closer to the critical point (where in the ulimate example we have only considered the additional case $(2, 2)$). Observe the astonishingly paral-

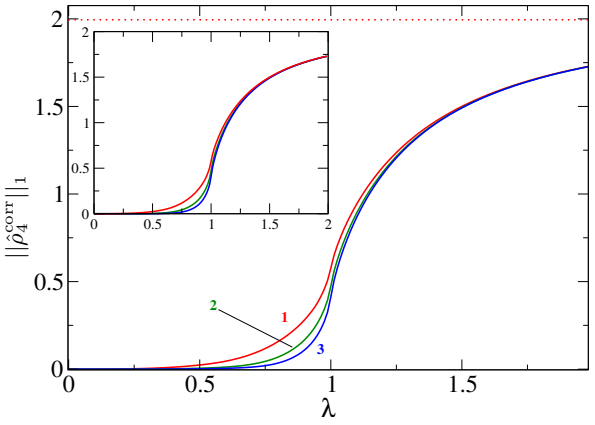

FIG. S7: $\|\hat{\rho}_4^{\rm corr}\|_1$ is shown for distances corresponding to $(1, d_2, 1)$ for $d = 1$ (red, 1) to 3 (blue, 3). The effect of growing d seems to be that the curve for d be an upper limit to m with $m < n$. The major change is done around the critical value of $J_c = 1$. The inset shows the distances $(2, 1, 2)$ and $(2, 2, 2)$ as compared to $(1, 1, 1)$. There is not much difference noted.

lel situation to the two-site case, namely that $\|\hat{\rho}_3^{\rm corr}(d_1, d_2)\|_1$ doesn't change so drastically with growing distance. This continues to hold for $\|\hat{\rho}_4^{\rm corr}(d_1, d_2, d_3)\|_1$ (see Fig. S7).

Difference in the norm

We have seen that the 1-norm serves as an upper bound to the correlation functions in the model. We nevertheless studied also the 2-norm, known as the Hibert-Schmidt or Frobenius norm. The result is shown in Fig S8. It is seen that the 2-norm close to the crtitical point $\hat{\rho}_4^{\rm corr}(1, 1, 1)$ is still considerably larger than $\hat{\rho}_3^{\rm corr}(1, 1)$; it is however still smaller than $\hat{\rho}_2^{\rm corr}(1)$ showing only a partial reordering. The corresponding eigenvalues of the matrices $\hat{\rho}_q^{\rm corr}(1)$, $q = 2, 3, 4$ is shown in Fig. S9.

RESULTS FOR THE BOSE-HUBBARD MODEL

The ground state of the Hamiltonian (4) is obtained numerically for arbitrary J by exact diagonalization in the subspace of the Hilbert space where the total momentum is zero. This allows to calculate exactly the reduced density matrices. In the basis of the occupation numbers $n_1 \dots n_q$, the entries $\langle n_1 \dots n_q|\hat{\rho}_q(d_1, \dots, d_{q-1})|n'_1 \dots n'_q\rangle$ do not vanish, provided that $\sum_{i=1}^q n_i = \sum_{i=1}^q n'_i = n_{\rm B} = 0, \dots, N$. Thus, the reduced density matrices possess a block-diagonal structure and the blocks are labeled by $n_{\rm B}$. The correlated density matrices have a similar structure.

The eigenvalues of the correlated reduced density operators $\hat{\rho}_q^{\rm corr}(1, \dots, 1)$ are shown in Fig. S10. With the increase of the number of lattice sites q, the number of nonvanishing eigenvalues grow but their magnitudes decrease. This leads to a qualitatively different behavior of the one- and two-norms that

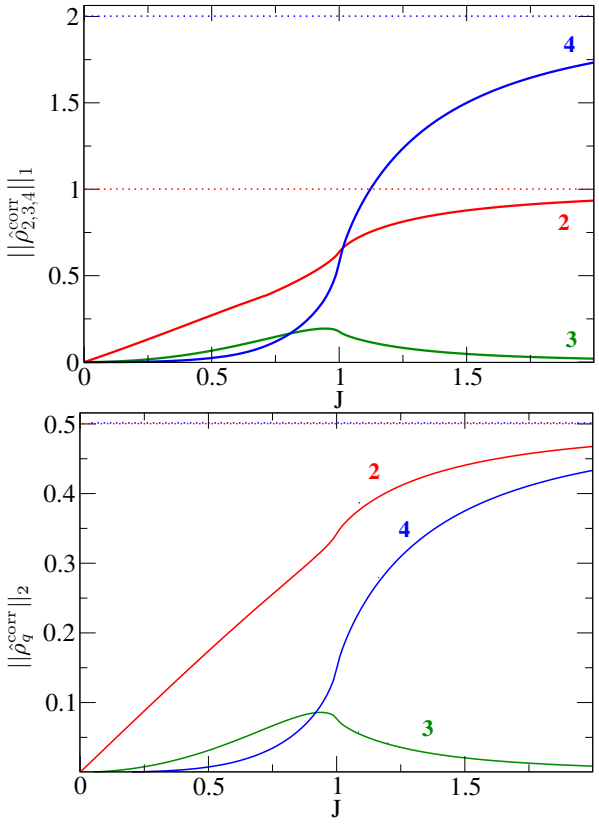

FIG. S8: Norms of correlated reduced density operators $\hat{\rho}_2^{\rm corr}(1)$ (red,2), $\hat{\rho}_3^{\rm corr}(1, 1)$ (green,3), $\hat{\rho}_4^{\rm corr}(1, 1, 1)$ (blue,4) for the ground state of the transverse Ising model. (a) 1-norms. For $J \lesssim 0.8$, $||\hat{\rho}_2^{\rm corr}(1)||_1 > ||\hat{\rho}_3^{\rm corr}(1, 1)||_1 > ||\hat{\rho}_4^{\rm corr}(1, 1, 1)||_1$. For $0.8 \lesssim J \lesssim 1$, $||\hat{\rho}_2^{\rm corr}(1)||_1 > ||\hat{\rho}_4^{\rm corr}(1, 1, 1)||_1 > ||\hat{\rho}_3^{\rm corr}(1, 1)||_1$. For $J \gtrsim 1$, $||\hat{\rho}_4^{\rm corr}(1, 1, 1)||_1 > ||\hat{\rho}_2^{\rm corr}(1)||_1 > ||\hat{\rho}_3^{\rm corr}(1, 1)||_1$. (b) 2-norms. $||\hat{\rho}_2^{\rm corr}(1)||_2$ is always larger than $||\hat{\rho}_3^{\rm corr}(1, 1)||_2$ and $||\hat{\rho}_4^{\rm corr}(1, 1, 1)||_2$. For $J \lesssim 0.9$, $||\hat{\rho}_4^{\rm corr}(1, 1, 1)||_2 < ||\hat{\rho}_3^{\rm corr}(1, 1)||_2$, and for $J \gtrsim 0.9$ we have the opposite.

are plotted in Fig. S11. The one-norms $||\hat{\rho}_q^{\rm corr}(1, \dots, 1)||_1$ grow monotonically with the increase of J and tend to finite constant values in the limit $J \to \infty$. For small values of J, we indeed have (S6) but already at moderate values of J the one-norms for different q become comparable to each other. It is quite surprising that $||\hat{\rho}_4^{\rm corr}(1, 1, 1)||_1$ becomes quickly larger than $||\hat{\rho}_3^{\rm corr}(1, 1)||_1$ and later also larger than $||\hat{\rho}_2^{\rm corr}(1)||_1$. This happens much before the critical point $J_{\rm c}$ of the superfluid–Mott-insulator transition. Hence we observe the same behavior as for the integrable Ising model.

The two-norms $||\hat{\rho}_q^{\rm corr}(1, \dots, 1)||_2$ display completely different behavior because the contribution of small eigenvalues is suppressed. The inequalities (S6) are satisfied for the two-norms at any value of J, although the difference between $q = 2, 3, 4$ is not very large near and above $J_{\rm c}$. The two-norms possess broad maxima and approach their asymptotic values at $J \to \infty$ from above.

If we consider one- and two-norms for fixed q but vary the distances between the sites, we find that both norms decrease

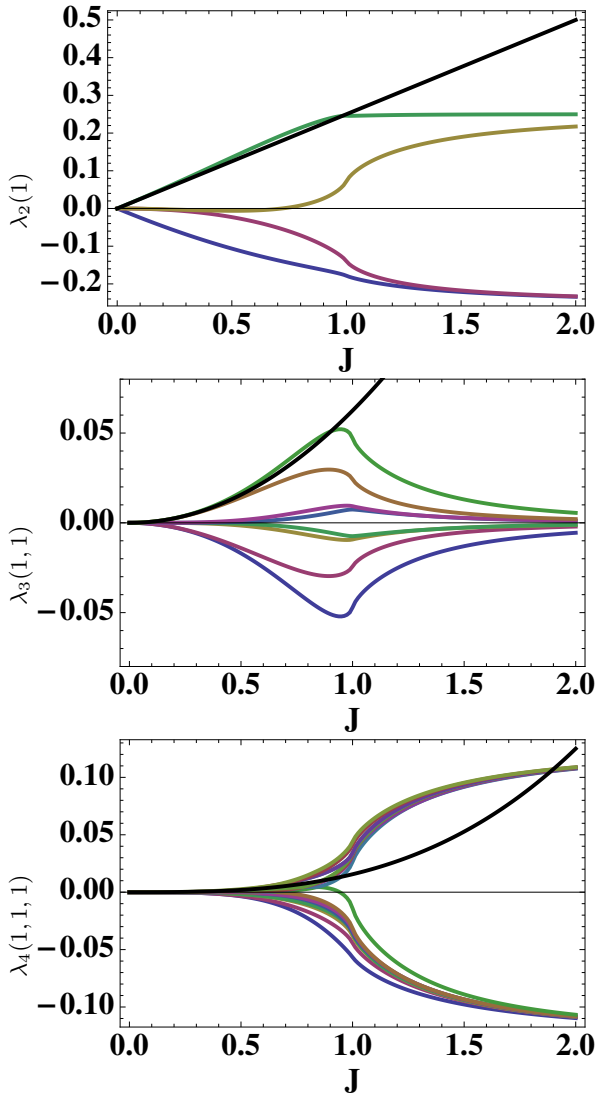

FIG. S9: Eigenvalues of the correlated reduced density operators $\hat{\rho}_2^{\rm corr}(1)$ (a), $\hat{\rho}_3^{\rm corr}(1,1)$ (b), $\hat{\rho}_4^{\rm corr}(1,1,1)$ (c) for the ground state of the transverse Ising model.

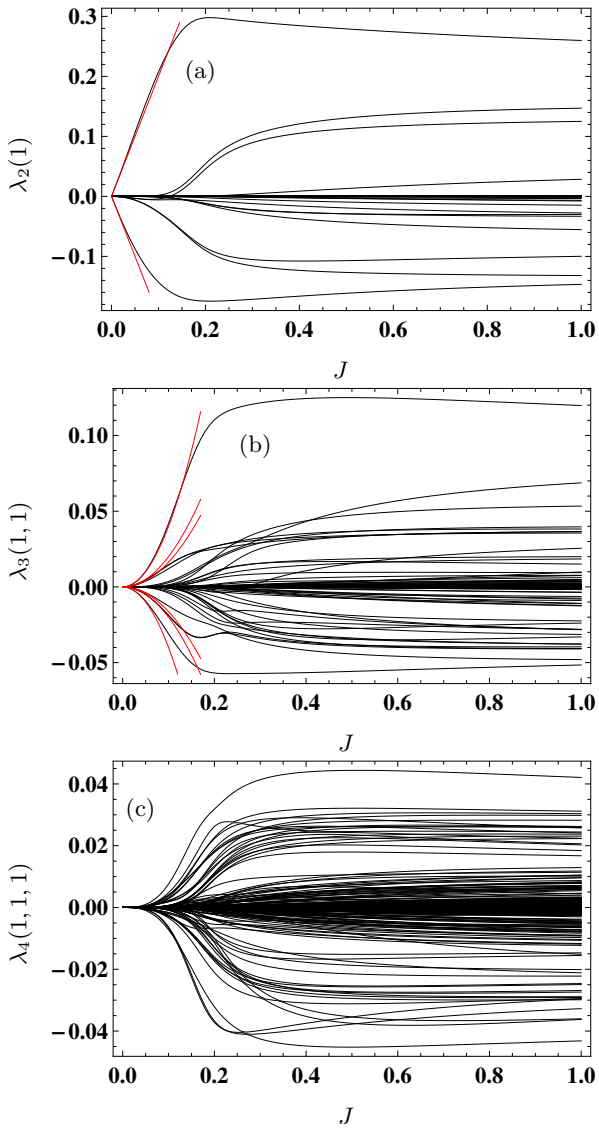

FIG. S10: Eigenvalues of the correlated reduced density operators $\hat{\rho}_2^{\rm corr}(1)$ (a), $\hat{\rho}_3^{\rm corr}(1,1)$ (b), $\hat{\rho}_4^{\rm corr}(1,1,1)$ (c) for the ground state of the Bose-Hubbard model. Black lines – exact diagonalization for $N = L = 12$. Red lines – strong-coupling expansion, see Eqs. (S8).

with the distance which is demonstrated in Fig. S12 for two sites ($q = 2$). The same was also observed for the transverse Ising model.

The correlated reduced density matrices can be calculated analytically for small values of J, employing the strong-coupling expansion [7]. In the leading order of J, this gives the following results for their nonvanishing eigenvalues

$$\begin{aligned}
\lambda_2^{(\pm 1)}(1) &\approx \pm\sqrt{2n(n+1)}\,J\,, \\
\lambda_2^{(\pm 1)}(2) &= \lambda_2^{(\pm 2)}(2) \approx \pm n(n+1)\,J^2\,, \\
\lambda_2^{(\pm 2)}(2) &\approx \pm(2n+1)\sqrt{2n(n+1)}\,J^2\,, \\
\lambda_3^{(\pm 1)}(1,1) &\approx \pm 2n(n+1)\,J^2\,, \\
\lambda_3^{(\pm 2)}(1,1) &= r_3^{(\pm 3)}(1,1) \approx \pm n(n+1)\,J^2\,, \\
\lambda_3^{(\pm 4)}(1,1) &\approx \pm\frac{2}{3}\sqrt{n(n+1)(2n^2+2n-1)}\,J^2\,,
\end{aligned} \tag{S8}$$

where $n = N/L$ is assumed to be an arbitrary integer. Then

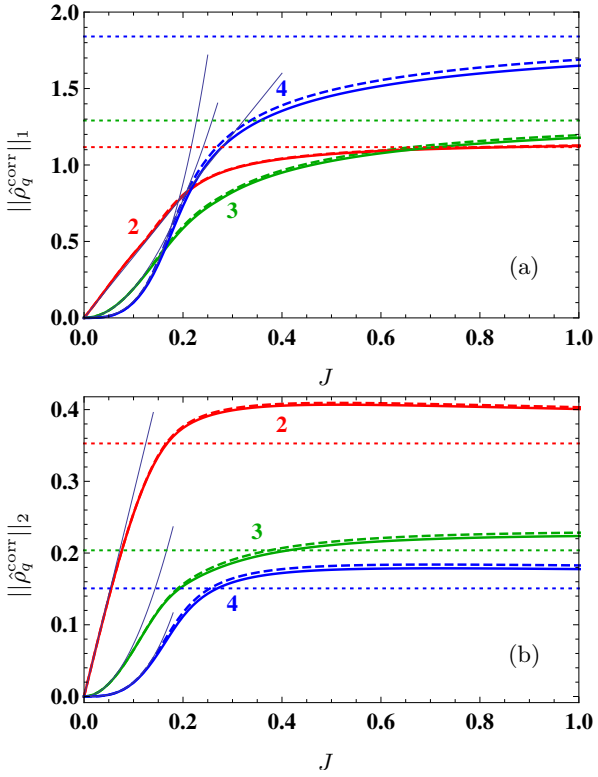

FIG. S11: Norms of correlated reduced density operators $\hat{\rho}_2^{\rm corr}(1)$ (red,2), $\hat{\rho}_3^{\rm corr}(1,1)$ (green,3), $\hat{\rho}_4^{\rm corr}(1,1,1)$ (blue,4) for the ground state of the Bose-Hubbard model. The results of exact diagonalization are shown by dashed curves for $N = L = 9$ and by solid curves for $N = L = 12$. Horizontal dotted lines - the limit of the ideal Bose gas ($J \to \infty$, $N = L = 12$). Thin solid lines – strong-coupling expansion [Eq. (S10)].

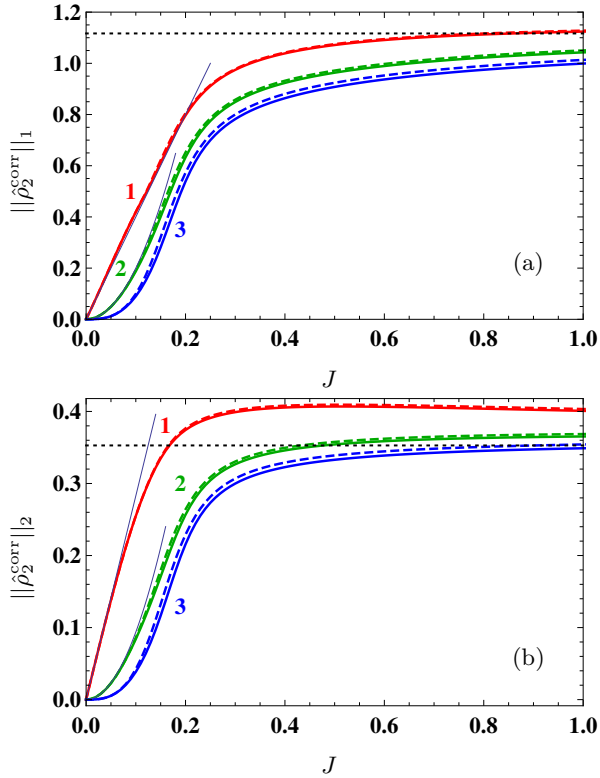

FIG. S12: Norms of correlated reduced density operators $\hat{\rho}_2^{\rm corr}(1)$ (red,1), $\hat{\rho}_2^{\rm corr}(2)$ (green,2), $\hat{\rho}_2^{\rm corr}(3)$ (blue,3) for the ground state of the Bose-Hubbard model. The results of exact diagonalization are shown by dashed curves for $N = L = 9$ and by solid curves for $N = L = 12$. Horizontal dotted lines - the limit of the ideal Bose gas ($J \to \infty$, $N = L = 12$). Thin solid lines – strong-coupling expansion [Eq. (S9)].

for the norms we get

$$
\begin{aligned}
||\hat{\rho}_2^{\rm corr}(1)||_1 &\approx 2\sqrt{2n(n+1)}\,J\,, \\
||\hat{\rho}_2^{\rm corr}(1)||_2 &\approx 2\sqrt{n(n+1)}\,J\,, \\
||\hat{\rho}_2^{\rm corr}(2)||_1 &\approx 2\left[2n(n+1)\right. \\
&\quad \left.+(2n+1)\sqrt{2n(n+1)}\right]J^2\,, \\
||\hat{\rho}_2^{\rm corr}(2)||_2 &\approx 2\sqrt{n(n+1)(5n^2+5n+1)}\,J^2\,, \\
||\hat{\rho}_3^{\rm corr}(1,1)||_1 &\approx \left[8n(n+1)\right. \\
&\quad \left.+\frac{4}{3}\sqrt{n(n+1)(2n^2+2n-1)}\right]J^2\,, \\
||\hat{\rho}_3^{\rm corr}(1,1)||_2 &\approx \frac{2}{3}\left\{n(n+1)\left[31n(n+1)-2\right]\right\}^{1/2}J^2\,.
\end{aligned}
\tag{S9}
$$

In the special case $n = 1$, this gives

$$
\begin{aligned}
&||\hat{\rho}_2^{\rm corr}(1)||_1 \approx 4J\,, \quad ||\hat{\rho}_2^{\rm corr}(1)||_2 \approx 2.82J\,, \\
&||\hat{\rho}_3^{\rm corr}(1,1)||_1 \approx 19.266J^2\,, \quad ||\hat{\rho}_3^{\rm corr}(1,1)||_2 \approx 7.3J^2\,,
\end{aligned}
\tag{S10}
$$

which is in excellent agreement with our numerical calculations (see Fig. S11).

In the limit of the ideal Bose gas ($J \to \infty$), the entries of the reduced density matrices depend only on the number of sites q but not on the distances between those:

$$
\begin{aligned}
\langle n_1 \ldots n_q|\hat{\rho}_q|n_1' \ldots n_q'\rangle &= \frac{N!}{(N-n_{\rm B})!n_{\rm B}!}\left(\frac{n_{\rm B}!}{n_1!\ldots n_q!}\right)^{1/2} \\
&\times \left(\frac{n_{\rm B}!}{n_1'!\ldots n_q'!}\right)^{1/2}\left(1-\frac{q}{L}\right)^{N-n_{\rm B}}\left(\frac{1}{L}\right)^{n_{\rm B}}\,.
\end{aligned}
\tag{S11}
$$

Eq. (S11) leads to rather simple expressions for the 2-norms in the thermodynamic limit

$$
\begin{aligned}
||\hat{\rho}_2^{\rm corr}||_2 &= \left[I_0(4\langle\hat{n}_\ell\rangle) - I_0^2(2\langle\hat{n}_\ell\rangle)\right]^{1/2} e^{-2\langle\hat{n}_\ell\rangle}\,, \\
||\hat{\rho}_3^{\rm corr}||_2 &= [I_0(6\langle\hat{n}_\ell\rangle) - 3I_0(2\langle\hat{n}_\ell\rangle)I_0(4\langle\hat{n}_\ell\rangle) \\
&\quad + 2I_0^3(2\langle\hat{n}_\ell\rangle)\Big]^{1/2} e^{-3\langle\hat{n}_\ell\rangle}\,,
\end{aligned}
$$

where $\langle\hat{n}_\ell\rangle = N/L$ is not necessarily an integer and $I_0(x)$ is the modified Bessel function of the first kind. For $\langle\hat{n}_\ell\rangle = 1$, this yields $||\hat{\rho}_2^{\rm corr}||_2 \approx 0.334$, $||\hat{\rho}_3^{\rm corr}||_2 \approx 0.184$. These values are slightly lower than those shown in Fig. S11(b) indicated by the horizontal dotted lines, which is a manifestation of the finite-size effects.

[1] F. Verstraete, M. Popp, and J. I. Cirac, Phys. Rev. Lett. **92**, 027901 (2004).
[2] A. Acín, A. Andrianov, E. Jane, and R. Tarrach, J. Phys. A **34**, 6725 (2001).
[3] H. A. Carteret, A. Higuchi, and A. Sudbery, J. Math. Phys. **41**, 7932 (2000).
[4] D. Ž. Đoković and A. Osterloh, J. Math. Phys. **50**, 033509 (2009).
[5] P. Pfeuty, Ann.Phys. **57**, 79 (1970).
[6] M. Hofmann, A. Osterloh, and O. Gühne, Phys. Rev. B **89**, 134101 (2014).
[7] J. K. Freericks and H. Monien, Phys. Rev. B **53**, 2691 (1996).